Chapter 3

Orbital Ordering of Manganese Oxides

3.1 Orbital Polarization in LaSrMnO$_4$

3.1.1 Introduction

Unlike the magnetic ordering or spin polarization, experimental methods to distinguish between spin and orbital polarization are limited. And direct observation of the orbital ordering has been known to be difficult. In order to establish the concept of the orbital ordering, the experimental measurements is indispensable. Recently, developments of synchrotron radiation as a brilliant source of polarized x-ray, x-ray absorption spectroscopy and resonant x-ray scattering (RXS) have attracted studies of valence orbital states, especially in d- and f-electron systems.

Measurements of resonant x-ray scattering at the Mn $1s$ threshold have been demonstrated for the evidence of $3d$-orbital ordering of manganites [7, 8]. In one of the interpretations of RXS measurements, a Mn $1s$ electron is first excited to the unoccupied Mn $4p$-state by absorbing the incident pho-

ton and then a photon is emitted resulting from the $4p \rightarrow 1s$ de-excitation. Consequently the ordering of $4p$-orbitals, *e.g.*, the alternately arrangement of $4p_x$ and $4p_y$ orbitals of Mn in LaMnO$_3$, is directly observed. Through intraatomic $3d - 4p$ multipole interaction, ordering of Mn $3d$-orbitals is indirectly observed. However such an interpretation of RXS at Mn K-edge is controversial. Orbital ordering in transition-metal oxides is typically accompanied by Jahn-Teller lattice distortion. Calculations based on a local-density approximation including on-site Coulomb interactions (LDA+U) [9, 10] and multiple scattering theory [11] indicate that RXS measurements pertain mainly to Jahn-Teller distortion, instead of directly observing $3d$ orbital ordering. To identify the orbital character of $3d$-states in orbital-ordered manganites is an important subject.

Polarization-dependent soft x-ray absorption, particularly linear dichroism, provides us with a powerful means to identify spin and orbital occupation of transition-metal oxides. For example, linear dichroism in XAS measurements on V$_2$O$_3$ enabled important observations on its electronic structure, identifying the orbital occupation of V $3d^2$ ions in various phases, suggesting that they are in a high-spin state, *i.e.,* S $= 1$ [4].

Calculations based on a single-ion model which includes the $3d$-$3d$ and $3d$-$2p$ multipole interactions and a crystal field have recently shown that the linear dichroism in Mn $L_{2,3}$ absorption exhibits multiplet structure and strongly reflect $3d$-orbital polarization, but insensitive to the Jahn-Teller distortion of the crystal [5, 6]. Linear dichroism therefore is expected to be a
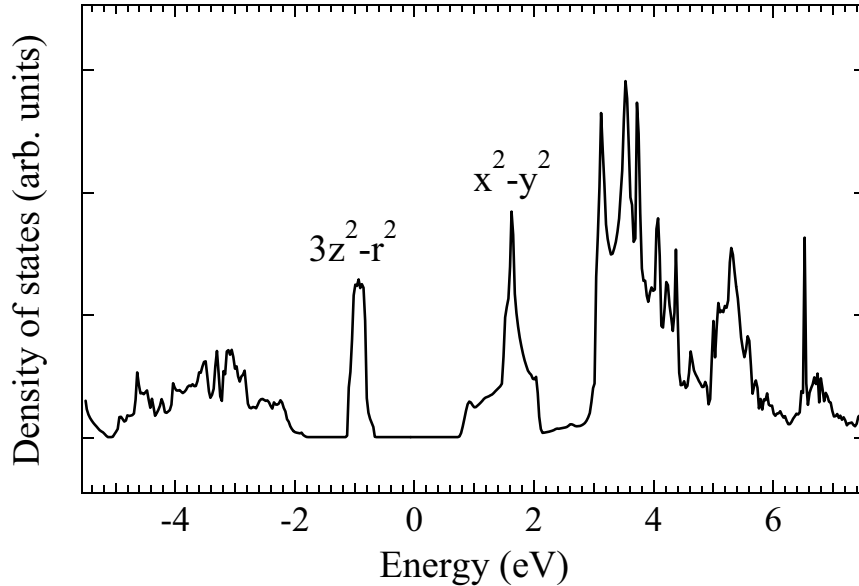
Figure 3.1: Partial density of states of Mn $3d$ in LaSrMnO$_4$ obtained from LDA+U calculations with U = 8 eV. The Fermi level is the zero of energy.

promising method to identify the orbital character of $3d$-electrons of orbital ordered compounds.

3.1.2 Theoretical Calculations

We used a cluster model based on a configuration interaction (CI) approach to calculate XAS and linear dichroism spectra of LaSrMnO$_4$ [13, 14]. In the calculation, octahedral MnO$_4^{5-}$ clusters were used. Because of strong Mn $3d$ - O $2p$ hybridization, the electronic state of the Mn^{3+} ions is described as a linear combination of the $3d^4$, $3d^5\underline{L}$, $3d^6\underline{L}^2$, where $\underline{L}$ denotes a hole on oxygen $2p$ orbital. We calculated the spectra by exactly diagonalizing the single-ion Hamiltonian under the crystal field where multipole interactions between the $3d$-$3d$ and $3d$-$2p$ core are described by the Slater integrals and the spin-orbit

interactions. The "non multiplet" Hamiltonian describing valence and core states and the effective interaction between electrons are expressed in terms of the 3d-3d and 3d-2p Coulomb interactions (U_{dd} and U_{dc}, respectively), and the hybridization strength between Mn 3d and O 2p. In addition, the charge fluctuation between the ligand 2p and cation 3d is also taken into account with charge-transfer energy Δ defined as $(E_{3d^5\underline{L}} - E_{3d^4})$, where $E_{3d^5\underline{L}}$ and E_{3d^4} are the average energies of $3d^5\underline{L}$ and $3d^4$ configurations, respectively.

The Hatree-Fock values were adopted for the coupling constants of the 2p-core and 3d spin-orbit interactions and 80% of the values were used for the Slater integrals, which describe the 3d-3d and 3d-2p multiplet interactions in the Hamltonia [15, 16]. The values of charge-transfer energy Δ, on-site Coulomb energies U_{dd} and U_{dc}, and hopping integrals ($V(t_{2g})$ and $V(e_g)$) between 3d and oxygen 2p molecular orbitals were included to reproduce the experimental spectra. In addition, we also used octahedral crystal field parameter $10Dq = \varepsilon_d(e_g) - \varepsilon_d(t_{2g})$, and hybridization strength between the O 2p orbitals $2T_{pp} = \varepsilon_L(e_g) - \varepsilon_L(t_{2g})$ as the calculation parameters. To reduce the number of the free parameters, the empirical relation between Slater-Koster hopping integrals $pd\sigma \approx -4/\sqrt{3}pd\pi$ was assumed.

3.1.3 Experimental Results

Single-crystalline samples of LaSrMnO$_4$ were grown by the floating zone method, as described elsewhere [17]. Measurements of x-ray diffraction at room temperature show that our samples are of single phase and
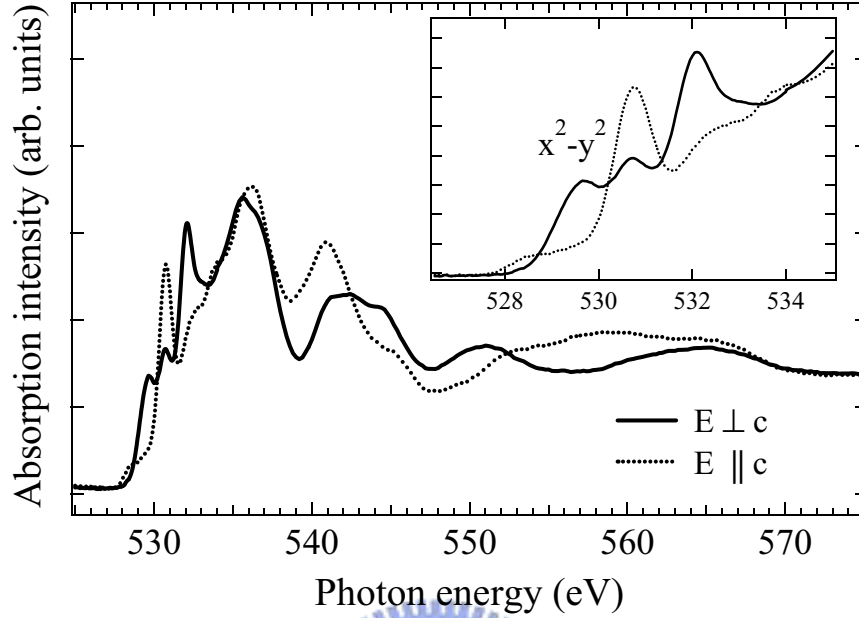
Figure 3.2: Polarization-dependent O 1s XAS of LaSrMnO$_4$ single crystal. The solid and dashed lines show the spectra taken with the **E** vector of photons perpendicular and parallel to the crystal c-axis.

have the $I4/mmm$ tetragonal structure with lattice constants c=13.04 Å and a=3.81 Å. The crystal also exhibits Jahn-Teller distortion, $i.e.$, the Mn-O bond length of 2.29 Å along the c-axis and 1.90 Å along the a-axis and b-axes.

XAS measurements on LaSrMnO$_4$ single crystals at various temperatures were performed at the Dragon beamline of the National Synchrotron Radiation Research Center in Taiwan. We recorded XAS spectra by collecting the sample drain current at 300 K. Crystals were $in\text{-}situ$ cleaved in an ultra-high vacuum at 90 K; the incident angle was 60° from the sample surface normal and the photon energy resolution was 0.2 eV.

To experimentally confirm the strong 3d-orbital polarization of LaSrMnO$_4$

concluded from LDA+U band structure calculations, we performed O 1s
XAS. Absorption at the oxygen K-edge is a dipole allowed transition in
which an O 1s electron is excited to unoccupied O 2p orbitals. The pre-edge
structure, *i.e.*, the structure at the absorption threshold, is determined by
the hybridization between O 2p and Mn 3d bands. In addition, at slightly
higher energies, the XAS structure is determined unoccupied orbitals cor-
responding to the hybridization between the oxygen and the La 4f/5d and
Sr 3d orbitals. In configuration approach, the strength of O 1$s \rightarrow$ 2p tran-
sition of LaSrMnO$_4$ is determined by the weight of 3$d^5\underline{L}$ character in the
ground state. Polarization-dependent O 1s XAS therefore reflects the sym-
metry of unoccupied Mn 3d orbitals. Figure 3.2 depicts O 1s XAS spectra
of LaSrMnO$_4$ with the **E** vector of photons perpendicular and parallel to the
crystal c-axis. Our measurements reveal that the lowest unoccupied O 2p
bands have a strong in-plane character, consistent with the conclusion ob-
tained from LDA+U calculations, indicating that LaSrMnO$_4$ exhibits $x^2 - y^2$
orbital character in its unoccupied e_g band. It is interesting to note that the
pre-edge results of our O 1s measurements are nearly identical to those of
previous measurements with *in-situ* cleaved samples [18], but in contrast to
those of specially cut samples with annealing under Ar atmosphere [19].

Figure 3.3 shows the polarization-dependent XAS spectra of LaSrMnO$_4$
taken with the **E** vector of photons perpendicular ($\mathbf{E} \perp c$) and parallel ($\mathbf{E} \parallel c$)
to the crystal c-axis. Since the unoccupied e_g band has a strong orbital
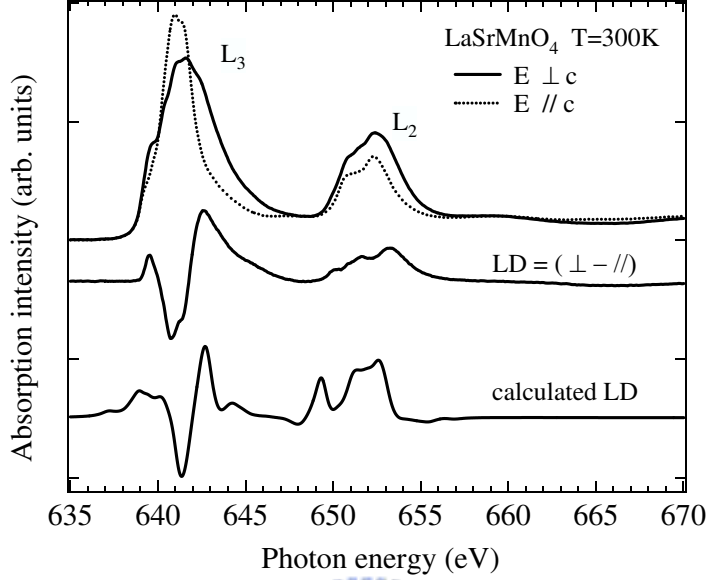anisotropy, the cross section of Mn 2$p \rightarrow$ 3d absorption excited by photons

Figure 3.3: Measured LD and polarization-dependent XAS taken with $\mathbf{E} \perp c$ (solid line) and $\mathbf{E} \parallel c$ (dashed line) of LaSrMnO$_4$. Bottom is the calculated LD spectrum of Mn^{3+} ions with occupied $d_{3z^2-r^2}$ orbitals.

with in-plane polarization ($\mathbf{E} \perp c$) is larger than that with out-of-plane polarization ($\mathbf{E} \parallel c$), if the multiplet effect resulting from $3d - 3d$ and $2p - 3d$ multipole interactions is neglected. In L_3 region, the four core $2p$-states contribute to $3d - 2p$ multipole interaction and multiplet structures, while the two states in L_2 region. The difference in XAS between the two linear polarizations is therefore remarkable in L_3 region compared with L_2 region. By an inspection of $2p-3d$ multipole interaction described by the Gaunt coefficient, the XAS spectral width for E perpendicular to c-axis is found to be larger than that for E parallel to c-axis both in L_3 and L_2, if $3z^2 - r^2$ is occupied. This causes the basic LD feature especially in L_3, although less prominent in L_2. Our measurements of linear dichroism indeed show that the integrated
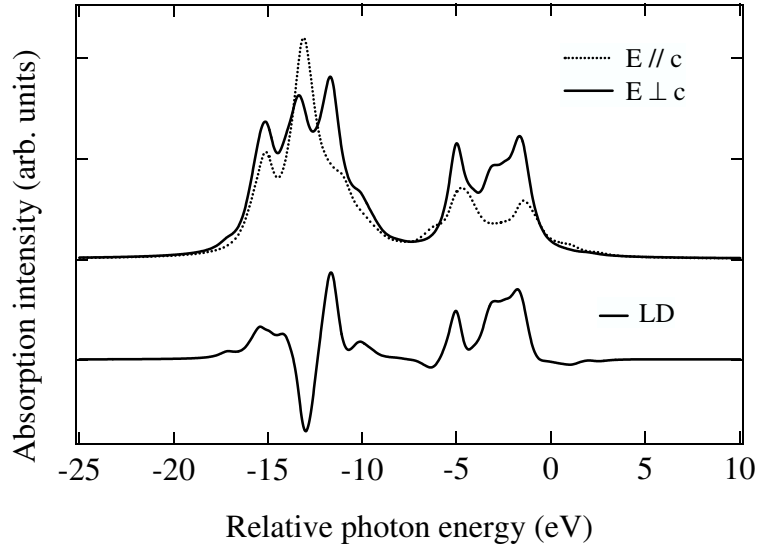
Figure 3.4: Calculated LD and polarization-dependent XAS of Mn^{3+} with $3d_{3z^2-r^2}$. The solid and dashed lines show the spectra taken with the **E** vector of photons perpendicular and parallel to the crystal c-axis.

intensity of XAS taken with in-plane polarization is larger than that with out-of-plane polarization, consistent with the above argument.

To further understand the LD spectrum of LaSrMnO$_4$, we performed multiplet calculations to obtain polarization dependent XAS. In our calculations, we assumed $10Dq = 2.2\ eV$. Other paparameters are the same as those used in Ref. [5]. We used parameters Δ_i and Δ_f to represent the energy difference between $3d_{3^2-r^2}$ and $3d_{x^2-y^2}$ orbitals in the initial and the final states of XAS, respectively; we assumed that $3d_{3^2-r^2}$ has lower energy than $3d_{x^2-y^2}$ for Δ_i and Δ_f positive. Δ_i and Δ_f result from the contribution of the molecular field and the Jahn-Teller distortion; the former is $\sim$ 0.1 eV at temperature below the transition, while the latter can be several tenth of an eV. By comparing the LD spectra of different values of Δ_i and Δ_f, we

found that the LD spectrum is weakly dependent on Δ_f and the basic feature of LD spectrum is determined by $3d$ electron distribution in the initial state. In other words, LD is insensitive to the Jhan-Teller distortion of the MnO$_6$ cluster [60]. With $\Delta_i = 0.1$ eV, and $\Delta_f = 0.5$ eV, Figure 3.4 shows calculated LD and polarization-dependent XAS of Mn^{3+} with $3d_{3z^2-r^2}$ orbital occupied; the spectra taken with $\mathbf{E} \perp c$ and $\mathbf{E} \parallel c$ are plotted by solid and dashed lines, respectively. Most of the features in the measured LD at Mn L-edge are reproduced by multiplet calculations for Mn^{3+} ions with occupied $d_{3z^2-r^2}$ orbitals, revealing that LD in L-edge XAS is an effective means to examine the orbital character of $3d$ electronic states in an orbital-ordered compound.

The comparison of measurements of polarization-dependent XAS with multiplet calculations leads us to suggest that one can use LD in L-edge x-ray absorption to identify the nature of orbital ordering in transition metal compounds such as the orbital nature of half-doped single-layered manganites which exhibit CE-type antiferromagnetic ordering and charge-orbital ordering [20, 17, 21, 7]. Below a charge ordering temperature T$_{CO}$=217 K, the valence of La$_{0.5}$Sr$_{1.5}$MnO$_4$ orders in an alternating pattern with two distinct sites identified as Mn^{3+} and Mn^{4+} [17, 21]. Electron-lattice coupling and Coulomb correlations give rise to alternating orbital ordering. In contrast to the $3z^2 - r^2$ "ferro-orbital" ordering in LaSrMnO$_4$, e_g electrons of the Mn^{3+} sites in La$_{0.5}$Sr$_{1.5}$MnO$_4$ are believed to exhibit an orbital ordering of $3x^2 - r^2/3y^2 - r^2$, in which occupied $d_{3x^2-r^2}$ and $d_{3y^2-r^2}$ orbitals are alternately arranged at two sublattices in the ab plane. However, $d_{3x^2-r^2}$ and

$d_{x^2-z^2}$ ($d_{3y^2-r^2}$ and $d_{y^2-z^2}$) orbitals might be mixed, because orbitals of these two types have the same spatial symmetry in the MnO$_2$ plane. Next section, we apply the technique of LD in soft x-ray absorption to clarify the orbital character of 3d electrons in the Mn e_g band of La$_{0.5}$Sr$_{1.5}$MnO$_4$. Furthermore, in principle, we should able to directly observe both orbital ordering and Jahn-Teller ordering in manganites by using LD in resonant x-ray scattering at Mn L$_{2,3}$-edges.

3.1.4 Conclusion

We have studied the orbital polarization of 3d electrons in the Mn e_g band of LaSrMnO$_4$. The results demonstrate that LD in Mn 2p XAS is a powerful method to test the validity of models for orbital ordering in transition-metal oxides. This technique would open up a new avenue for determining the orbital character of 3d electrons in transition metal oxides, and possibly examining the mechanism of orbital ordering.

3.2   Orbital Ordering in La$_{0.5}$Sr$_{1.5}$MnO$_4$

Orbital ordering is an important topic in research of transition-metal oxides. The magnetic and transport properties of strongly electron correlation systems are closely related to the orbital and charge degrees of freedom [53]. In particular, charge-orbital ordering of half-doped manganites has attracted much attention [23-29]. We used the LD in Mn $2p$ XAS to study the orbital ordering in half-doped manganites.

3.2.1   Introduction

La$_{1-x}$Sr$_{1+x}$MnO$_4$ has single-layer perovskite structure (or so-called K$_2$NiF$_4$ structure) as shown in Figure 3.5(A). The composition x in this formula represents the nominal hole number per Mn site. The Mn^{3+} valance state (LaSrMnO$_4$; $x = 0$) is viewed as the parent compound.

Figure 3.5(B) shows the temperature dependence of resistivity and magnetic susceptibility for single crystals of La$_{1-x}$Sr$_{1+x}$MnO$_4$ with various hole concentrations [30]. A steep increase in resistivity is observed near 220 K for x=0.5. Comparing with the anomalies in the resistivity, magnetic susceptibility, and electron diffraction studies [30], the superlattice peaks arise from the charge-ordered state. More directly, Sternlieb *et al.* [31] studied the single-crystalline with neutron scattering which provides evidence for the charge and spin order in MnO$_2$ plane. The charge shows the alternating pattern with two distinct sites identified as Mn^{3+}/Mn^{4+} in the MnO$_2$ plane below the transition temperature of charge-ordering(CO) $T_{CO} = 217$
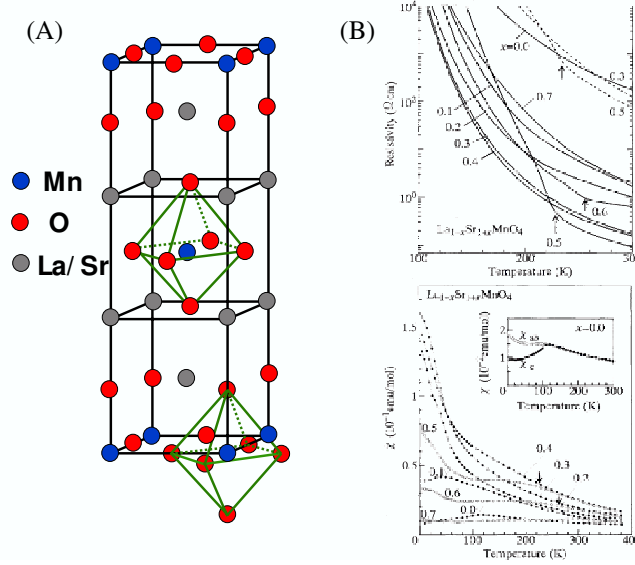
Figure 3.5: (A): The single-layered perovskite structure of manganites.   (B): Temperature dependence of resistivity and magnetic susceptibility for single crystals of La$_{1-x}$Sr$_{1+x}$MnO$_4$. (from Ref. [30]) Solid and dash curves are for the in-plane(ρ_{ab}) and the out-of-plane(ρ_c) components, respectively.

K, as shown in left panel of Figure 3.6. Below the Nèel temperature, $T_N = 110$ K, the magnetic moments form an ordered structure with a unit cell of $2\sqrt{2}a \times 2\sqrt{2}a \times 2c$.

La$_{0.5}$Sr$_{1.5}$MnO$_4$ exhibits CE-type ordering. The CE-type spin ordered pattern for the pseudo-cubic perovskite is displayed in Fig. 3.6. Half-doped La$_{0.5}$Sr$_{1.5}$MnO$_4$ also exhibits charge and orbital ordering; the e_g electron on the nominal Mn^{3+} sites of La$_{0.5}$Sr$_{1.5}$MnO$_4$ are believed to exhibit an orbital ordering of $3x^2$-$r^2/3y^2$-r^2. As displayed in Figure 3.7, the occupied $d_{3x^2-r^2}$ and $d_{3y^2-r^2}$ orbitals are alternately arranged at two sublattices in the ab plane. The La$_{0.5}$Sr$_{1.5}$MnO$_4$ has a zigzag-chain magnetic structure. The magnetic moments of Mn on the chain form a ferromagnetic coupling, but
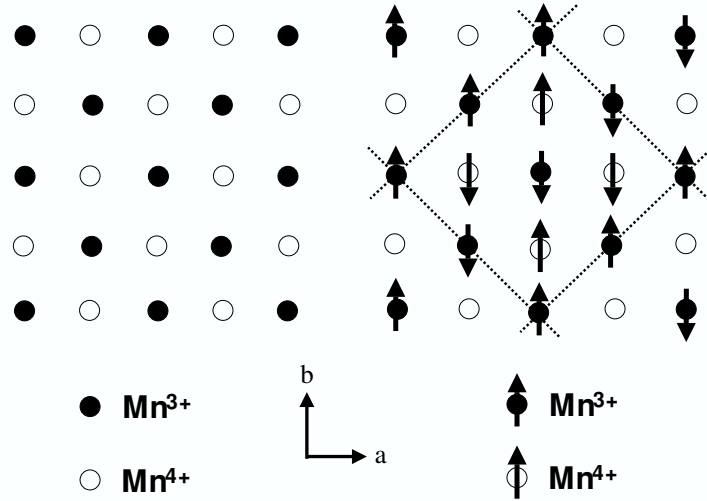
Figure 3.6: Schematic view of charge ordering (left panel) and antiferromagnetic ordering pattern (rught panel) of La$_{0.5}$Sr$_{1.5}$MnO$_4$. Only Mn^{3+} and Mn^{4+} ions are displayed.

antiferromagnetic coupling between the zigzag chains.

This type of charge/orbital ordering has been measured by Murakami *et al.* [32] with resonant hard x-ray scattering at Mn K-edge. However, to observe orbital ordering directly is a difficult task. Experimental results of resonant hard x-ray scattering at the Mn K-edge in La$_{0.5}$Sr$_{1.5}$MnO$_4$ show removal of degeneracy between $4p_x$ and $4p_y$. This kind of observations is controversial. Orbital ordering in transition metal oxides is typically accompanied by Jahn-Teller lattice distortion. And resonant hard x-ray scattering measurements pertain mainly to Jahn-Teller distortion, instead of directly observing 3d-orbital ordering.

On the other hand, the $d_{3x^2-r^2}$ and $d_{x^2-z^2}$ ($d_{3y^2-r^2}$ and $d_{y^2-z^2}$) orbitals might be mixed, because of these two types orbitals have the same spatial
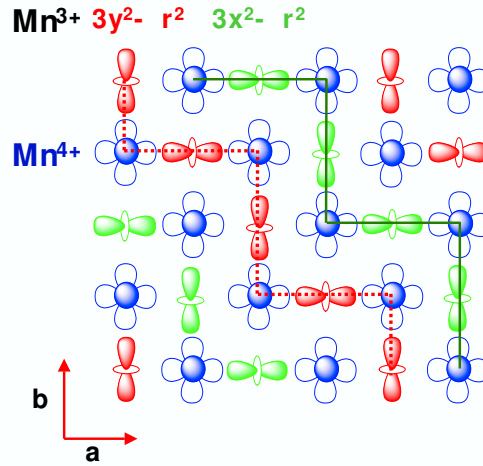
Figure 3.7: Schematic view of orbital ordering of half doped manganites: La$_{0.5}$Sr$_{1.5}$MnO$_4$. Only the Mn^{3+} and Mn^{4+} ions are displayed.

symmetry in the MnO$_2$ plane. To clarify the nature of orbital ordering in La$_{0.5}$Sr$_{1.5}$MnO$_4$, it is essential to reveal the origin of orbital-ordering in half-doped manganites.

Here, we present the linear dichroism measurements in Mn $2p$-edge XAS of La$_{0.5}$Sr$_{1.5}$MnO$_4$. The results of linear dichroism measurements are compared with multiplet calculations to unravel the orbital character of e_g states in La$_{0.5}$Sr$_{1.5}$MnO$_4$. Also the LDA+U calculations were used to study the orbital ordering of this compound.

3.2.2 Linear Dichroism
A. La$_{1-x}$Sr$_{1+x}$MnO$_4$ Samples

Single-crystalline samples of La$_{1-x}$Sr$_{1+x}$MnO$_4$ were grown by floating zone method [30]. X-ray diffraction measurements at room temperature show

the single phase of our samples. The major crystallographic difference between different concentrations (x) is the lattice constance in the c-axis. This length decreases significantly from 13.04 Å for x=0 to 12.43 Å for x=0.5. Whereas the a-axis length shows only a weak x dependence(3.81 Å for x=0 to 3.86 Å for x=0.5). The difference of the c-axis length is attributed to a significantly decreased out-of-plane Mn-O bond length with increasing Sr content. Crystals were freshly cleaved in an ultrahigh vacuum at 90K temperature.

B. Mn L-edge XAS

As shown in figure 3.8(a), the LD in XAS on La$_{1-x}$Sr$_{1+x}$MnO$_4$ with varied doping clarify the origin of the LD signal. Because the Jahn-Teller effect on the Mn^{4+} ions is insignificant [38, 39], the contribution of 3d-orbitals of these ions to LD is much smaller than that of Mn^{3+} ions. The LD magnitude of doped La$_{1-x}$Sr$_{1+x}$MnO$_4$ diminishes with increasing the Sr doping, which is proportional to the decreases of Mn^{3+} ions. The magnitude of LD decreases more rapidly than that from a simple picture of Mn^{3+}/Mn^{4+} dilution. In particular, the LD magnitude of La$_{0.5}$Sr$_{1.5}$MnO$_4$ is $\sim \frac{1}{4}$ that observed from LaSrMnO$_4$, and the sign at the L_2-edge is the same as that in LaSrMnO$_4$.

To identify the orbital character of the occupied e_g states. We used the model of MnO$_6$ cluster based on configuration interaction to calculate the LD spectra of Mn^{3+} ions with $d_{x^2-z^2}/d_{y^2-z^2}$ and $d_{3x^2-r^2}/d_{3y^2-r^2}$ orbitals occupied, as shown in figure 3.8(b) [41]. Overall the calculated LD of occupied in-
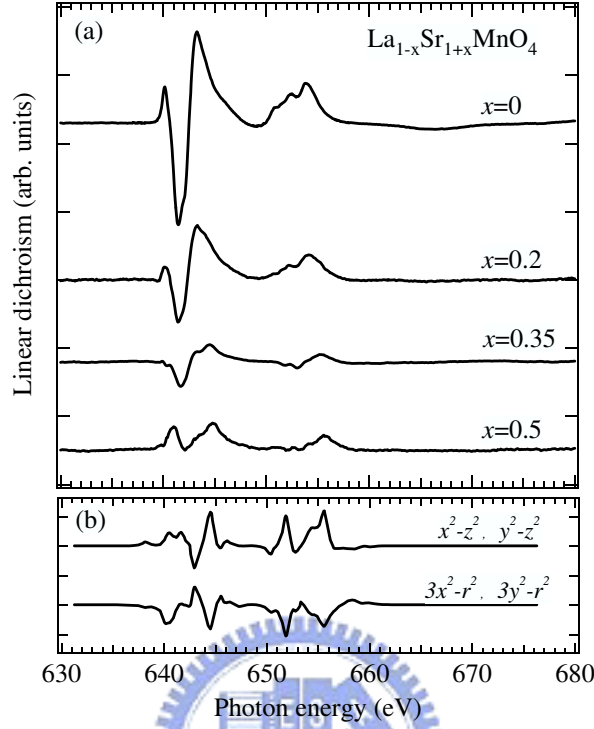
Figure 3.8: (a) LD in Mn $L_{2,3}$-edge XAS of La$_{1-x}$Sr$_{1+x}$MnO$_4$ with varied Sr doping. Linear dichroism spectra were derived from XAS normalized to the same peak intensity at Mn L_3-edge and measured at 300K for $x \ll 0.35$ and 150K for x=0.5. (b) The multiplet calculated LD spectra of Mn^{3+} ions with $d_{x^2-z^2}/d_{y^2-z^2}$ and $d_{3x^2-r^2}/d_{3y^2-r^2}$ orbital occupied in e_g state.

plane orbitals such as $d_{3x^2-r^2}/d_{3y^2-r^2}$ is with sign reversed to that of out-of-plane orbitals such as $d_{x^2-z^2}/d_{y^2-z^2}$. The conventional orbital-ordering model of $3x^2 - r^2/3y^2 - r^2$ type is incompatible with LD measurements. Comparing with the LD measurements from La$_{0.5}$Sr$_{1.5}$MnO$_4$, the calculated LD of $3x^2 - r^2/3y^2 - r^2$ type orbital ordering has reversed sign with the measurement result. One might suspect this inconsistency could result from anisotropic e_g charge distribution on the Mn^{4+} sites. If so, only e_g charge with $d_{3z^2-r^2}$ or $d_{x^2-z^2}/d_{y^2-z^2}$ polarization transferred from Mn^{3+} to Mn^{4+} could give rise to a LD similar to the measurement. However, even in the

most unfavorable case, that is, even if the transferred e_g charge on the Mn^{4+} site were maximum (leading to equal charges on both Mn sites) and fully $(3z^2 - r^2)$-polarized, only half of the observed LD could be accounted for. As shown later (see the lower panel of Fig. 3.11), such transferred e_g charges indeed have a small in-plane polarization. This anisotropy gives opposite contributions to LD with respect to the measurement; the inconsistency can not be reconciled even if the anisotropic charge distribution of Mn^{4+} was taken into account.

Furthermore, the lineshape of the measured LD spectrum for $x = 0.5$ is similar to those from calculations for Mn^{3+} with occupied $d_{3z^2-r^2}$ or $d_{x^2-z^2}$ / $d_{y^2-z^2}$ orbitals, implying that La$_{0.5}$Sr$_{1.5}$MnO$_4$ has an orbital polarization of strong z character, e.g., $d_{3z^2-r^2}$ or $d_{x^2-z^2}/d_{y^2-z^2}$. If La$_{0.5}$Sr$_{1.5}$MnO$_4$ exhibited $3z^2 - r^2$ orbital ordering, all Mn^{3+} sites, i.e., half of all Mn atoms, would contribute to LD and its magnitude at Mn L_2-edge would be half of that observed in LaSrMnO$_4$, in contrast to the measurements. If La$_{0.5}$Sr$_{1.5}$MnO$_4$ exhibits $x^2 - z^2/y^2 - z^2$ orbital ordering, by choosing LD as the difference in XAS spectra taken with the **E** vector parallel to x and z axes, we observe essentially linear dichroism resulting only from the sublattice with occupied $d_{y^2-z^2}$. In other words, only half of Mn^{3+} sites contribute to LD; one quarter of Mn atoms contribute to LD, consistent with the measurements. Our LD measurements thus suggest that orbital ordering of the e_g states on the Mn site in La$_{0.5}$Sr$_{1.5}$MnO$_4$ is dominated by $x^2 - z^2/y^2 - z^2$ type.

In addition, measurements of temperature-dependent linear dichroism of

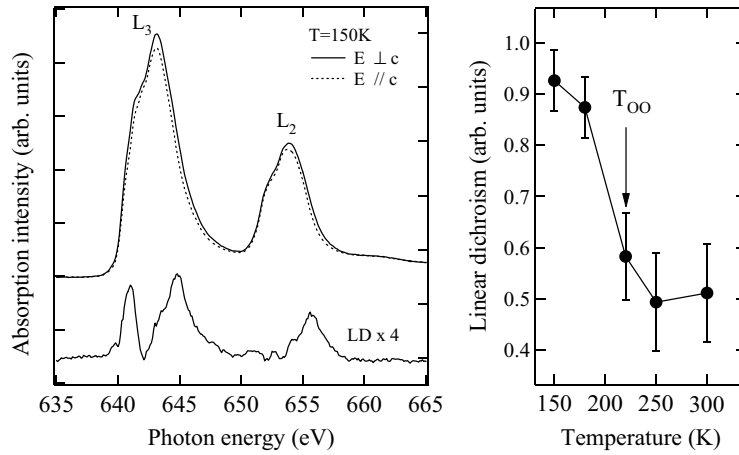Figure 3.9: Left panel: XAS and LD spectra of La$_{0.5}$Sr$_{1.5}$MnO$_4$ recorded at temperatures 150 K. Right panel: temperature dependence of relative LD in XAS measured at temperatures about T$_{CO}$. The solid line is for visual guidance. Error bars reflect uncertainties from different sets of data.

La$_{0.5}$Sr$_{1.5}$MnO$_4$ about T$_{CO}$ provide us with further evidence that LD in XAS reflects the nature of orbital ordering. LD measurements with photon energy of 645 eV show that the LD decreases greatly as the temperature crosses T$_{CO}$, as shown in Fig. 3.9, indicating that orbital ordering of La$_{0.5}$Sr$_{1.5}$MnO$_4$ follows a similar temperature-dependent trend of charge ordering [31] and Jahn-Teller distortion [32]. To confirm this, more detailed temperature dependent studies would be necessary.

B. O K-edge XAS

After establishing the orbital characters of the occupied electronic states of La$_{0.5}$Sr$_{1.5}$MnO$_4$, we measured polarization-dependent O 1s XAS to further explore the orbital symmetry in La$_{1-x}$Sr$_{1+x}$MnO$_4$. In O K-edge XAS, the $1s \rightarrow 2p$ transition is determined by the $3d^{n+1}\underline{L}$ configuration in the ground state of $3d^n$. Polarization-dependent O K-edge XAS could provide us the
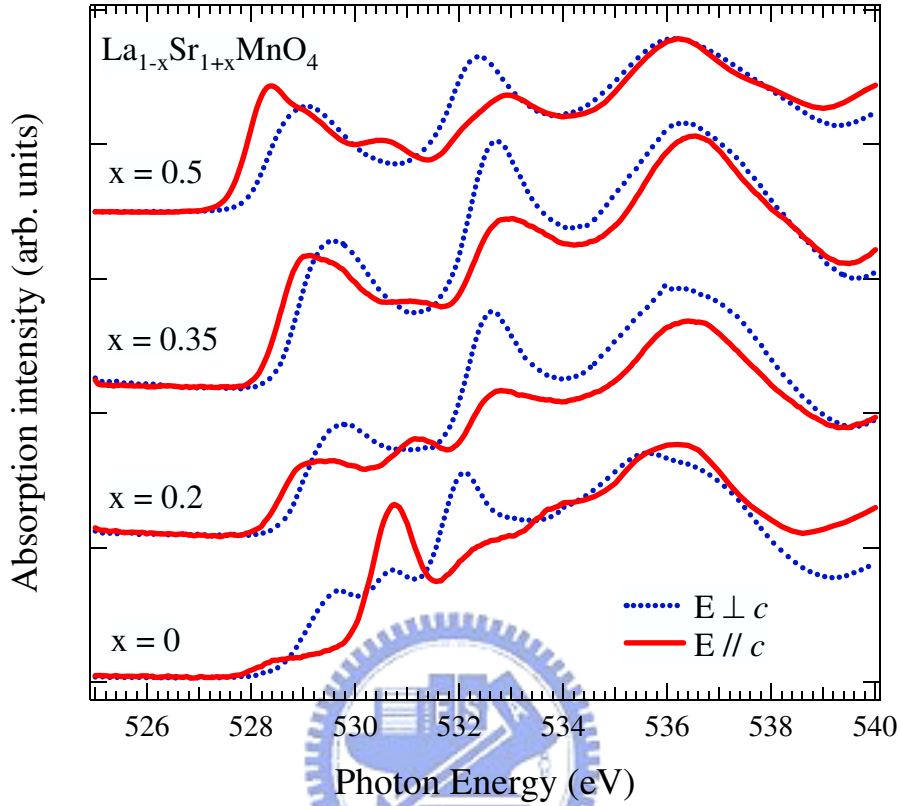
Figure 3.10: Polarization dependent O K-edge XAS of La$_{1-x}$Sr$_{1+x}$MnO$_4$ with various Sr dopings.

information about orbital symmetry in the unoccupied Mn $3d$ states.

Figure 3.10 shows the polarization-dependent O K-edge XAS spectra of La$_{1-x}$Sr$_{1+x}$MnO$_4$ with various Sr dopings. At photon energy 529.6 eV, the polarization-dependent XAS spectra with $\mathbf{E} \perp c$ and $\mathbf{E} \parallel c$ reveal that the lowest unoccupied O $2p$ bands of LaSrMnO$_4$ have an in-plane character, indicating that LaSrMnO$_4$ exhibits $x^2 - y^2$ orbital character in the unoccupied e_g band. With increase of the Sr doping to 0.2, the absorption intensity increases at the pre-edge (at 528.9 eV) of the O K-edge XAS with $\mathbf{E} \parallel c$, indicating that the low energy excitation has an out-off-plane orbital charac-

ter. When the Sr doping reaches to 0.35, the pre-edge absorption intensity with $\mathbf{E} \parallel c$ increases further. The composition x represents the hole number per Mn site in La$_{1-x}$Sr$_{1+x}$MnO$_4$ and x is proportional to the population of Mn^{3+} cations. In ionic picture, the Mn^{3+}/Mn^{4+} dilution is $(1-x)/x$. The Mn^{3+} is in the $(t_{2g})^3(e_g)^1$ configuration. In contrast, there is no e_g electron existing on the Mn^{4+} cation. Because of the hybridization between Mn $3d$ and O $2p$, the electronic state of the Mn^{4+} is described as a linear combination of $3d^3$, $3d^4\underline{L}$, and $3d^5\underline{L}^2$. In configuration approach, the O $1s \rightarrow 2p$ transition in La$_{1-x}$Sr$_{1+x}$MnO$_4$ is determined by the weight of $3d^4\underline{L}$ character in the ground state. As the Sr doping increases from x=0.35 to x=0.5, the XAS spectra show a rigid-band shift which means the photon energy of absorption threshold decreases. In the band picture, the number of occupied e_g electron decreases with Sr doping which makes the necessary absorption energy in $1s \rightarrow 2p$ transition decreasing. This rigid-band shift associated with e_g bands is determined by the position of the Fermi level.

3.2.3 LDA+U Calculations

To further study orbital ordering in La$_{0.5}$Sr$_{1.5}$MnO$_4$, we performed LDA+U calculations using the full-potential linearized augmented-plane-wave method on La$_{0.5}$Sr$_{1.5}$MnO$_4$ in CE-type AFM structure with U and J equal to 8 and 0.88 eV for Mn $3d$ electrons, respectively [34]. Details of the calculations will be described elsewhere [42]. Mahadevan *et al.* [38] found that the breathing-type Jahn-Teller distortion of La$_{0.5}$Sr$_{1.5}$MnO$_4$ sug-

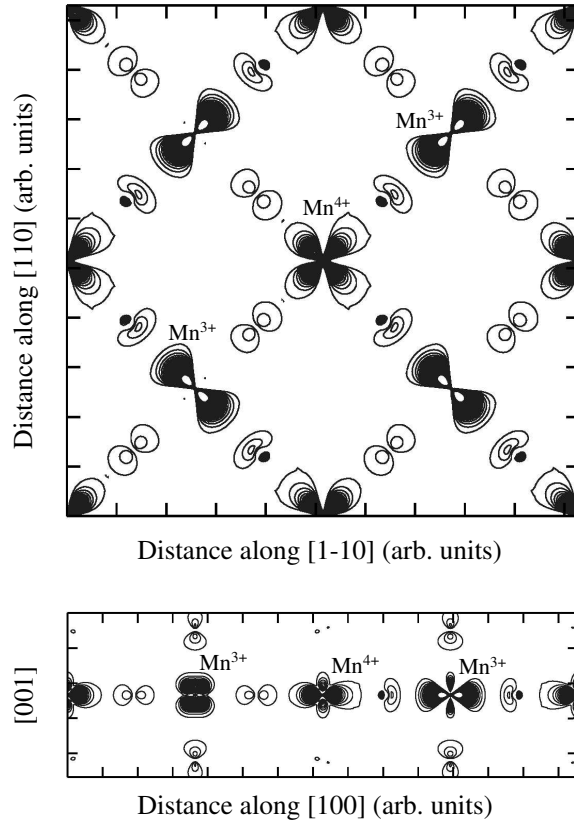Figure 3.11: Charge-density contours corresponding to the e_g valence bands of La$_{0.5}$Sr$_{1.5}$MnO$_4$. Upper panel: Charge-density contours in the *ab*-plane. Lower panel: Charge-density contours in the *ac*-plane along [100] direction. (from Ref. [12])

gested by Sternlieb *et al.* [31] is not energetically favorable, and proposed

a shear-type Jahn-Teller distortion in which the Mn-O length is elongated

alternately along the x and y directions. Measurements of x-ray scattering

also indicate a shear-type distortion on Mn-O octahedra [43], rather than a

breathing-type distortion. Consistent with previous band-structure calcula-

tions [38], our LDA+U calculations show also that La$_{0.5}$Sr$_{1.5}$MnO$_4$ without

Jahn-Teller distortion is unstable against a shear-type Jahn-Teller distor-

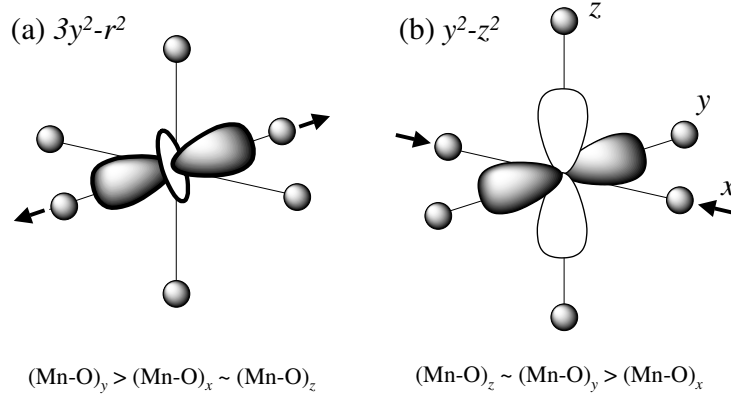tion. With a shear-type Jahn-Teller distortion of 0.08-Å in-plane O displace-

Figure 3.12: View of $d_{3y^2-r^2}$ and $d_{x^2-z^2}$ orbitals on the Mn^{3+} sites with different Jahn-Teller distortions. (a) and (b) show the Mn-O length elongated along the y direction and contracted along the x direction, respectively. Filled circles denote O atoms in which $2p$ orbitals are omitted for clarity.

ment [44], LDA+U calculations give rise to an orbital ordering dominated by $x^2 - z^2/y^2 - z^2$ on the Mn^{3+} sites of La$_{0.5}$Sr$_{1.5}$MnO$_4$, as shown in Fig. 3.11, which displays charge-density contours corresponding to the e_g dominated valence bands. Interestingly we found also that La$_{0.5}$Sr$_{1.5}$MnO$_4$ would exhibit $3x^2 - r^2/3y^2 - r^2$ orbital ordering if the on-site Coulomb interactions were not explicitly included, in agreement with previous LDA calculations [38]. Our results suggest that charge and orbital ordering can be well described if the on-site Coulomb interactions of $3d$-electrons are properly taken into account, as in the LDA+U or Hartree-Fock calculations. Such a cross-type orbital ordering results from a combined effect of AFM structure, Jahn-Teller distortion, and the on-site Coulomb interactions of $3d$-electrons.

The existence of orbital ordering of cross-type $x^2 - z^2/y^2 - z^2$ can be understood within the framework of crystal field effect with lattice distortion taken into account. On the Mn^{3+} sites of a cubic perovskite, e_g orbitals of

$3y^2-r^2$ $(3x^2-r^2)$ symmetry are preferentially occupied if the Mn-O length is elongated along the y (x) direction; y^2-z^2 (x^2-z^2) orbitals are occupied if the Mn-O length is contracted along the x (y) direction, as shown in Fig. 3.12. For example, in CE-type charge-orbital-ordered half-doped manganites of cubic perovskite such as La$_{0.5}$Ca$_{0.5}$MnO$_3$, the Mn^{3+} site exhibits a large Jahn-Teller distortion, in which the Mn-O length is elongated alternately along the x and y directions (two long bonds of 2.06 Å along the zigzag chain and four short bonds of 1.92 Å) [45], producing $3x^2-r^2/3y^2-r^2$ orbital ordering. As for La$_{0.5}$Sr$_{1.5}$MnO$_4$, the shear-type distortion leads effectively to alternate contractions of along the x and y directions in La$_{0.5}$Sr$_{1.5}$MnO$_4$, because the longer in-plane Mn-O length (2.00 Å) is close to the out-of-plane Mn-O length (1.98 Å), while the shorter in-plane Mn-O length is 1.84 Å. Orbital ordering of x^2-z^2/y^2-z^2 is expected to be energetically more favorable than that of $3x^2-r^2/3y^2-r^2$. Note that small tetragonal distortions with c/a=0.98 and c/a=1.04 in strained thin films of La$_{0.5}$Sr$_{0.5}$MnO$_3$ can result in ferro-orbital ordering of x^2-y^2 and $3z^2-r^2$, respectively [46, 47].

3.2.4 Conclusions

In conclusion, with LD measurements, we inferred that orbital ordering of the Mn e_g electrons in La$_{0.5}$Sr$_{1.5}$MnO$_4$ is dominated by x^2-z^2/y^2-z^2 type, as corroborated by our LDA+U calculations. Orbital ordering of Mn e_g electrons in La$_{0.5}$Sr$_{1.5}$MnO$_4$ results from a combined effect of antiferromagnetic structure, Jahn-Teller distortion, and on-site Coulomb interactions. In prin-

ciple, one can directly observe both orbital ordering and Jahn-Teller ordering

in manganites by using resonant x-ray scattering at Mn $L_{2,3}$-edges [48].

3.3 Strain Induced Orbital Polarization

3.3.1 Introduction

Manganese oxides $A_{1-x}B_x MnO_3$ (A stands for the trivalent rare-earth ions and B for the divalent alkaline earth ions) exhibit numerous exotic physical phenomena [49, 50, 51] and attract great interest from both experimental and theoretical points of view. The rich physical properties of these compounds arise from the strong coupling among spin, orbital, and charge degrees of freedom in maganites [52, 53]. In addition, the Jahn-Teller distortion of Mn^{3+} ions in these compounds plays an important role in the underlying physics of such exotic physical phenomena [54]. Particularly the strain effect in manganites are closely related to their magnetic and transport properties [55, 56, 57, 58]. These materials are also technologically important because the advent of synthetic maganites provides us with a great opportunities to control their phase.

Using the epitaxial strain, Konishi *et al.* demonstrated that magnetic and electronic phases of $La_{1-x}Sr_x MnO_3$ films can be controlled via changing lattice parameters of the substrates [56], suggesting that a small tetragonal distortion in strained thin films of $La_{0.5}Sr_{0.5}MnO_3$ can result in ferro-orbital ordering of $d_{x^2-y^2}$ or $d_{3z^2-r^2}$, depending upon the lateral strain, i.e., the value of c/a less or greater than 1. The epitaxial strain also leads to different spin structures. Figure 3.13 shows the spin structure and ferro-orbital ordering of $La_{0.5}Sr_{0.5}MnO_3$ films grown on $LaAlO_3$ and $SrTiO_3$ suggested by Konishi
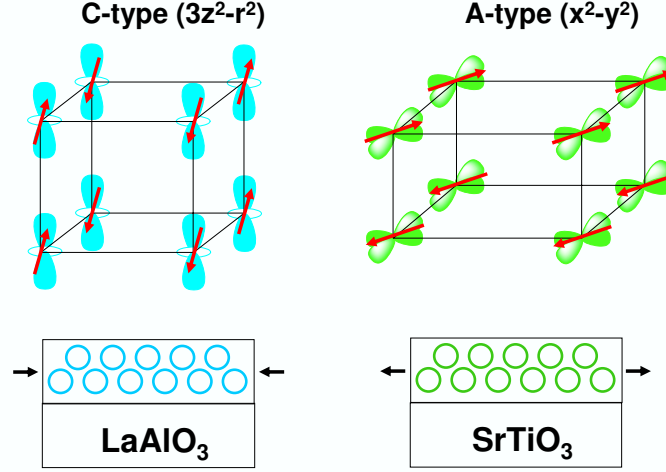
Figure 3.13: Illustrations of spin structures and ferro-orbital ordering of epitaxial $La_{0.5}Sr_{0.5}MnO_3$ thin films grown on $LaAlO_3$ and $SrTiO_3$ substrates. $La_{0.5}Sr_{0.5}MnO_3$ films with c/a grater and less than 1 exhibit, respectively, chain-type (C-type) and layer-type (A-type) antiferromagnetic structures and ferro-orbital ordering of $3z^2 - r^2$ and $x^2 - y^2$.

et al. In addition, such spin-orbital phases can be well explained by band-structure calculations based on the local density approximation (LDA) [59]. However, LDA calculations surprisingly predict that the e_g band of C-type AFM strained manganite films at the Fermi level has a stronger x^2-y^2 orbital character than $3z^2 - r^2$, although these films exhibit a ferro-orbital ordering of $d_{3z^2-r^2}$. Such a LDA prediction is in disagreement with the resistivity measurements that the C-type strained manganites is conductive only along the c-axis [56].

Here we demonstrate experimentally the existence of ferro-orbital ordered states resulting from tetragonal Jahn-Teller distortion by combining techniques of soft x-ray spectroscopy and synthesis of manganite thin films. To identify the orbital character of strained $La_{0.5}Sr_{0.5}MnO_3$ thin films, we
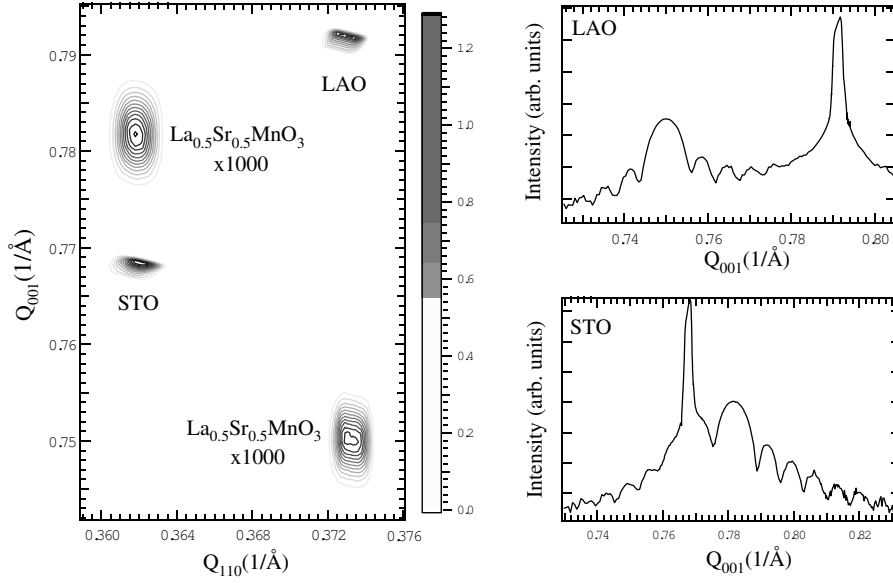
Figure 3.14: Left panel: The reciprocal-space mapping contour of the (113) x-ray Bragg diffraction peaks of $La_{0.5}Sr_{0.5}MnO_3$ epitaxial thin films on STO and LAO substrates. Right panel: Q_{001} scans, i.e., scans of momentum transfer along the c direction of the (113) Bragg diffraction peak with fixed in-plane momentum transfer Q_{110} along the [110] direction. Q_{110} is fixed at 0.3731 Å^{-1} and 0.3618 Å^{-1}, respectively, for Q_{001} scans of thin films deposited on LAO and STO.

measured polarization-dependent soft x-ray absorption on $La_{0.5}Sr_{0.5}MnO_3$

thin films grown epitaxially on $SrTiO_3$ (abbreviated hereafter as STO) and

$LaAlO_3$ (abbreviated hereafter as LAO) with the technique of pulsed laser

deposition (PLD) [63, 64].

3.3.2 Epitaxial Growth of $La_{0.5}Sr_{0.5}MnO_3$ Thin films

We used UV radiation of wavelength 248 nm from a KrF excimer laser

to achieve PLD for the growth of $La_{0.5}Sr_{0.5}MnO_3$ thin films epitaxially on

STO(001) and LAO(001). During the deposition of manganite thin films,

STO and LAO substrates were kept at 900 K in a background oxygen pressure

of 0.1 mTorr. The thickness of $La_{0.5}Sr_{0.5}MnO_3$ thin films is 200 Å. We carried

out x-ray diffraction (XRD) measurements to characterize the crystalline structure of $La_{0.5}Sr_{0.5}MnO_3$ thin films at the beamline 17A of NSRRC with photon energy of 9.3 KeV. Our measurements of XRD show that these films are epitaxial. The reciprocal-space mapping of the (113) Bragg diffraction from the samples are shown in Fig. 3.14. The diffraction spots from the substrate and the thin film have the same momentum transfer Q_{110} along the [110] direction, while the values of the out-of-plane momentum transfer Q_{001} are quite different. XRD results unravel that the in-plane lattice constant (a) of the thin film perfectly matches with that of the substrate, whereas the out-of-plane lattice constant (c) is compressed or elongated, depending upon the lattice parameter of substrates. The x-ray diffractions along the c axis, i.e., the Q_{001} scan, of the (113) peak are also plotted in Figure 3.14. These Q scans also show the pronounced fringes resulting from the interference of reflected beams from different interfaces. The well-defined values of Q_{110} and Q_{001} show that the thin films grow epitaxially on STO and LAO with a coherent strain. The c/a values are different among thin films grown on different substrates. We found that the values of c/a for films on LAO and STO are 1.055 and 0.982, respectively; these thin films exhibit tetragonal Jahn-Teller distortion with elongated and contracted Mn-O bond length along the c axis, respectively. The observed strain also results a drastic change in physical properties such as electronic structures discussed below.
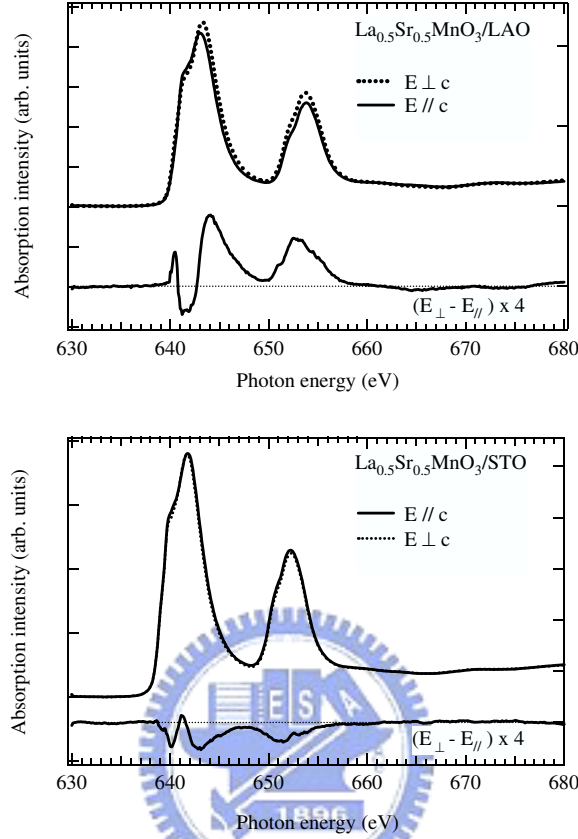
Figure 3.15: LD and polarization-dependent XAS taken with $\mathbf{E} \parallel c$ (solid line) and $\mathbf{E} \perp c$ (broken line) of $La_{0.5}Sr_{0.5}MnO_3$ thin films grown on STO and LAO.

3.3.3 Polarization-Dependent XAS

A. Mn L-edge XAS

Figure 3.15 shows the polarization-dependent Mn $2p$ XAS spectra of $La_{0.5}Sr_{0.5}MnO_3$ films on LAO taken with the $\mathbf{E}$ vector of photons perpendicular ($\mathbf{E} \perp c$) and parallel ($\mathbf{E} \parallel c$) to the crystal c axis. For the unoccupied e_g bands which have an orbital polarization of $x^2 - y^2$, the average cross section of Mn $2p \rightarrow 3d$ absorption excited by photons with out-of-plane polarization ($\mathbf{E} \parallel c$) is smaller than that with in-plane polarization ($\mathbf{E} \perp c$). In the L_3

region, four $2p$ states contribute to $3d - 2p$ multipole interaction and multi-plet structures, while there are two $2p$ states contributing to the absorption in the L_2 region. The difference in XAS between the two linear polarizations is therefore remarkable in the L_3 region compared with the L_2 region. By an inspection of $2p - 3d$ multipole interaction described by the Gaunt co-efficient, the XAS spectral strength for $\mathbf{E}$ perpendicular to c is found to be larger than that for $\mathbf{E}$ parallel to c both in the L_3 and L_2 regions, if $d_{3z^2-r^2}$ is occupied [60]. This causes the basic LD feature especially in L_3, although less prominent in L_2. Our measurements of linear dichroism of $La_{0.5}Sr_{0.5}MnO_3$ films on LAO indeed demonstrate that the integrated intensity of XAS taken with in-plane polarization is larger than that with out-of-plane polarization, thus revealing that the occupied e_g states of Mn are of $3z^2 - r^2$ symmetry.

In contrast, measurements of LD in XAS of $La_{0.5}Sr_{0.5}MnO_3$ films on STO show a polarization opposite to that of $La_{0.5}Sr_{0.5}MnO_3$ films on LAO, as depicted in the lower panel of Fig. 3.15, demonstrating that manganite films on $SrTiO_3$ are dominated by $d_{x^2-y^2}$ orbitals. The observations provide us with direct spectroscopic evidence that occupied Mn $3d$ states can be directly controlled by tetragonal Jahn-Teller distortion. One can interpret the lattice strain as a biasing field on the orbital state through Jahn-Teller channel; namely, the uniaxial strain with respect to the MnO_6 octahedron can serve as a pseudo field. As a result of the lattice mismatching with the substrates, the coherent lattice strain in epitaxial films of $La_{0.5}Sr_{0.5}MnO_3$ gives rise to different kinds of orbital-mediated phases. There is one e_g electron on the

nominal Mn^{3+} site, but no e_g electron exists on the nominal Mn^{4+} site. Tetragonal Jahn-Teller distortion lifts the degeneracy of $d_{3z^2-r^2}$ and $d_{x^2-y^2}$ orbitals in the e_g manifold. For strained half-doped $La_{0.5}Sr_{0.5}MnO_3$ films grown on STO, the highest occupied state has an orbital symmetry of x^2-y^2, while the $d_{3z^2-r^2}$ orbital is the highest occupied state in the films on LAO. These results lead us to suggest that the A-type AFM $La_{0.5}Sr_{0.5}MnO_3$ films with $c/a < 1$ is metallic in the ab plane, whereas the C-type AFM films with $c/a > 1$ is nonmatellic in the ab plane, in agreement with previous resistivity measurements [56].

B. O K-edge XAS

After establishing the orbital characters of the occupied electronic states of strained $La_{0.5}Sr_{0.5}MnO_3$ thin films, we measured O $1s$ XAS to further explore the orbital symmetry of electronic states responsible for the low-energy excitations in C-type AFM manganite films. X-ray absorption at the oxygen K-edge has been proved to be sensitive to the orbital symmetry of low-energy excitations in transition-metal oxides [65, 66]. In particular, the pre-edge structure, i.e., the structure at the absorption threshold, is determined by the hybridization between O $2p$ and Mn $3d$ bands and reflects the orbital symmetry of Mn $3d$. Namely, in the configuration approach, the strength of O $1s \rightarrow 2p$ transition is determined by the weight of $3d^n \underline{L}$ character in the ground state of $3d^n$, where n and $\underline{L}$ denote the number of Mn $3d$ electrons and a hole on the $2p$ orbital of oxygens, respectively. Polarization-dependent
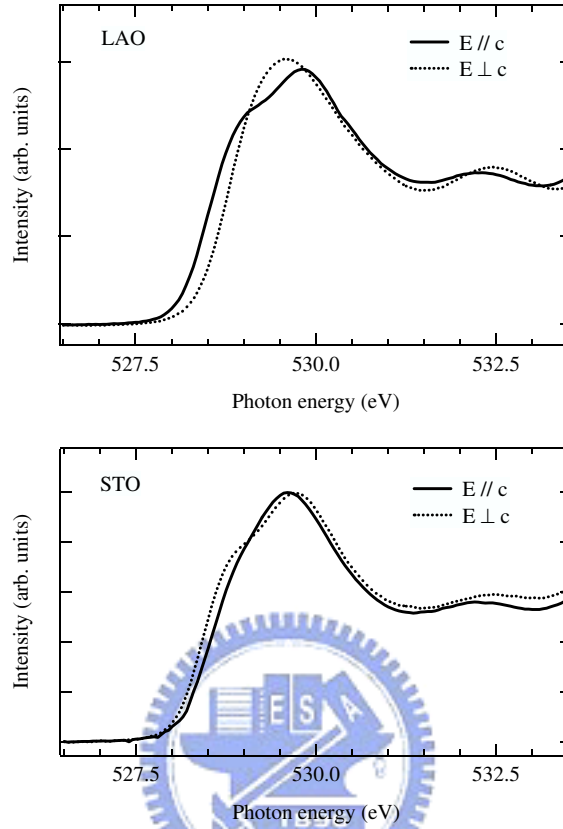
Figure 3.16: Polarization-dependent O K-edge XAS of strained $La_{0.5}Sr_{0.5}MnO_3$ thin films deposited on LAO and STO substrates. Solid and dashed lines are the spectra taken with the **E** vector of photons parallel and perpendicular to the crystal c axis, respectively.

O $1s$ XAS therefore reflects the symmetry of unoccupied Mn $3d$ orbitals.

Figure 3.16 displays O $1s$ XAS spectra of strained $La_{0.5}Sr_{0.5}MnO_3$ thin films grown on LAO and STO substrates. Our measurements with **E** $\perp c$ and **E** $\parallel c$ reveal that the lowest unoccupied O $2p$ bands of $La_{0.5}Sr_{0.5}MnO_3$ thin film deposited on STO have an in-plane character, indicating $x^2 - y^2$ orbital character in the unoccupied lowest-lying e_g band. On the other hand, $La_{0.5}Sr_{0.5}MnO_3$ films deposited on LAO substrate have an out-of-plane character, indicating $3z^2 - r^2$ orbital character in the unoccupied lowest-lying e_g

band. In other words, the e_g electrons responsible for the low-energy exci-
tations of C-type AFM $La_{0.5}Sr_{0.5}MnO_3$ are of $3z^2 - r^2$ symmetry, consistent
with the transport measurements that this compound is conductive along the
c axis rather than in the ab plane. However LDA calculations [59] predict
that the e_g band of at the Fermi level of C-type AFM $La_{0.5}Sr_{0.5}MnO_3$ has a
stronger $x^2 - y^2$ orbital character than $3z^2 - r^2$.

3.3.4   LDA+U Calculations

To reconcile this discrepancy, we performed band-structure calculations
in the LDA approximations explicitly including the on-site Coulomb inter-
actions of $3d$, i.e., LDA+U [67]. Our LDA calculations confirm previous
LDA prediction that the e_g band at the Fermi level has a stronger $x^2 - y^2$
orbital character than $3z^2 - r^2$, as in Figure 3.17(A) which plots projected
densities of states arising from the e_g band. Clearly previous LDA calcula-
tions are inconsistent with our O $1s$ XAS results. Such a discrepancy could
stem from that electron correlations are not properly included in the LDA
approximation. For example, previous studies of soft x-ray absorption show
that charge-orbital ordering of half-doped $La_{0.5}Sr_{1.5}MnO_4$ can not be well
described if the on-site Coulomb interactions of $3d$ electrons are not properly
taken into account [61]. As shown in Figure 3.17(B), our LDA+U calcula-
tions unravel that states of $x^2 - y^2$ symmetry pushed away from the Fermi
level by the Coulomb interactions; namely the e_g band at the Fermi level is
of $3z^2 - r^2$ symmetry, in agreement with transport measurements. Measure-
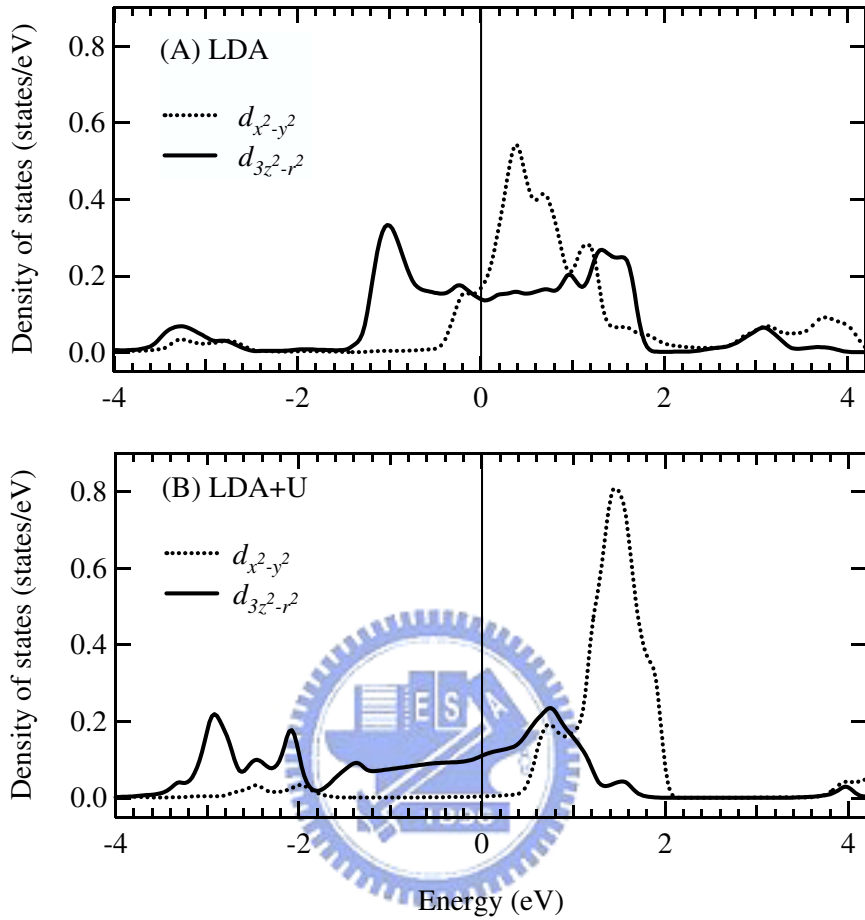
Figure 3.17: Projected densities of states arising from the e_g band of C-type AFM strained La$_{0.5}$Sr$_{0.5}$MnO$_3$ thin films with c/a=1.055 calculated in (A) LDA and (B) LDA+U approximations. The Fermi level is located at 0 eV.

ments of O 1s XAS and LDA+U calculations thus lead us to conclude that on-site Coulomb interactions are indispensable in describing orbital character of electronic states responsible for low-energy excitations in manganites, consistent with the conclusion of LD studies on La$_{0.5}$Sr$_{1.5}$MnO$_4$ [61].

3.3.5 Conclusions

In summary, we demonstrate that epitaxial thin films of $La_{0.5}Sr_{0.5}MnO_3$ with laterally compressed strain exhibit an orbital polarization of $3z^2 - r^2$, while those with laterally tensile strain has an orbital polarization of $x^2 - y^2$, consistent with the predictions from previous magnetization and resistivity measurements. Particularly we found that electronic states responsible for the low-energy excitations of C-type AFM $La_{0.5}Sr_{0.5}MnO_3$ films are dominated by $3z^2 - r^2$ symmetry, rather than $x^2 - y^2$ symmetry as predicted by LDA calculations, although the phase diagram can be explained from band-structure point of view. Compared with LDA+U calculations, our results indicate that such orbital polarizations in strained films of manganite result from a combined effect of tetragonal Jahn-Teller distortion and Coulomb interactions of Mn $3d$ electrons.

Reference

[1] G. E. Bacon, Neutron Diffraction, 3rd ed., Oxford University Press, (1975).

[2] K. I. Kugel and D. I. Khomskii, JETP Lett. **15**, 446 (1972).

[3] R. Shiina, H. Shiba, and P. Thalmeier, J. Phys. Soc. Jpn. **66**, 1741 (1997).

[4] J.-H. Park, L. H. Tjeng, A. Tanaka, J. W. Allen, C. T. Chen, P. Metcalf, J. M. Honig, F. M. F. de Groot, and G. A. Sawatzky, Phys. Rev. B **61**, 11506 (2000).

[5] H. B. Huang, T. Shishidou, and T. Jo, J. Phys. Soc. Jpn. **69**, 2399 (2000).

[6] H. B. Huang and T. Jo, J. Phys. Soc. Jpn., **71**, 3094 (2001).

[7] Y. Murakami, H. Kawada, H. Kawata, M. Tanaka, T. Arima, Y. Moritomo, and Y. Tokura, Phys. Rev. Lett. **80**, 1932 (1998).

[8] Y. Murakami, J.P. Hill, D. Gibbs, M. Blume, I. Koyama, M. Tanaka, H. Kawata, T. Arima, Y. Tokura, K. Hirota, and Y. Endoh, Phys. Rev. Lett. **81**, 582 (1998).

[9] I.S. Elfimov, V.I. Anisimov, and G.A. Sawatzky, Phys. Rev. Lett. **82**, 4264 (1999).

[10] P. Benedetti, J. van den Brink, E. Pavarini, A. Vigliante, and P. Wochner, Phys. Rev B **63**, 60408 (2001).

[11] M. Benfatto, Y. Joly, and C.R. Natoli, Phys. Rev. Lett. **83**, 636 (1999).

[12] G. Y. Guo *et al.* (unpublished).

[13] A. Tanaka and T. Jo, J. Phys. Soc. Jpn. **63**, 2788 (1994).

[14] A. Tanaka and T. Jo, J. Phys. Soc. Jpn. **61**, 2669 (1992).

[15] F. M. F. de Groot, J. C. Fuggle, B. T. Thole and G. A. Sawatzky, Phys. Rev. B **42**, 5459 (1990).

[16] T. Uozumi, K. Okada, A. Kotani, R. Zimmermann, P. Steiner, S. Hüfner, Y. Tezuka and S. Shin, J. Elect. Spect. Relat. Phenom. **83**, 9 (1997).

[17] Y. Moritomo, Y. Tomioka, A. Asamitsu, Y. Tokura, and Y. Matsui, Phys. Rev. B **51**, 3297 (1995).

[18] D. Dessau and Z.-X. Shen, in Colossal Magnetoresistive Oxides, Gordeorn and Breach Science Publishes, Ed. by Y. Tokura 149 (2000).

[19] Jan van Elp, Hitoshi Sato, Tsuyoshi Kimura, T. Toda, Y. Okamura, Yoshinori Tokura and Masaki Taniguchi, J. Phys. Soc. Jpn. **69**, 2391 (2000).

[20] J. B. Goodenough, Phys. Rev. **100**, 564 (1955).

[21] B. J. Sternlieb, J. P. Hill, U. C. Wildgruber, G. M. Luke, B. Nachumi, Y. Moritomo, and Y. Tokura, Phys. Rev. Lett. **76**, 2169 (1996).

[22] Y. Tokura and N. Nagaosa, Science **288**, 462 (2000).

[23] J. B. Goodenough, Phys. Rev. **100**, 564 (1955).

[24] E. O. Wollan and W. C. Koehler, Phys. Rev. **100**, 545 (1955).

[25] Y. Okimoto *et al.*, Phys. Rev. Lett. **75**, 109 (1995).

[26] P. Schiffer *et al.*, Phys. Rev. Lett. **75**, 3336 (1995).

[27] P. G. Radaelli *et al.*, Phys. Rev. B **55**, 3015 (1997).

[28] T. Mizokawa and A. Fujimori, Phys. Rev. B **56**, 493 (1997).

[29] S. Mori, C. H. Chen, and S. -W. Cheong, Nature (London) **392**, 3336 (1998).

[30] Y. Moritomo, Y. Tomioka, A. Asmitsu, Y. Tokura, and Y. Matsui, Phys. Rev. B **51**, 3297 (1995).

[31] B. J. Sternlieb, J. P. Hill, U. C. Wildgruber, G. M. Luke, B. Nachumi, U. Moritomo, and Y. Tokura, Phys. Rev. Lett. **76**, 2169 (1996).

[32] Y. Murakami, H. Kawada, H. Kuwata, M. Tanaka, T. Arima, Y. Moritomo, and Y. Tokura, Phys. Rev. Lett. **80**, 1932 (1998).

[33] Y. Murakami *et al.*, Phys. Rev. Lett. **81**, 582 (1998).

[34] I. S. Elfimov, V. I. Anisimov, and G. A. Sawatzky, Phys. Rev. Lett. **82**, 4264 (1999).

[35] P. Benedetti, J. van den Brink, E. Pavarini, A. Vigliante, and P. Wochner, Phys. Rev. B **63**, 60408 (2001).

[36] H. B. Huang, T. Shishidou, and T. Jo, J. Phys. Sco. Jpn. **69**, 2399 (2000).

[37] H. B. Huang and T. Jo, J. Phys. Sco. Jpn. **71**, 3094 (2001).

[38] P. Mahadevan, K. Terakura, and D. D. Sarma, Phys. Rev. Lett. **87**, 066404 (2001).

[39] Z. Popovic and S. Satpathy, Phys. Rev. Lett. **88**, 197201 (2002).

[40] J. van Elp and A. Tanaka, Phys. Rev B **60**, 5331 (1999).

[41] We used $U = 8.0$ eV, $10Dq = 2.0$eV, charge-transfer energy $\Delta = 2.1$ eV, and $pd\sigma = 2.1$eV.

[42] G. Y. Guo *et al.* (unpublished).

[43] S. Larochelle *et al.*, Phys. Rev. Lett. **87**, 95502 (2001).

[44] The longer and shorter in-plane Mn-O lengthes are, respectively, 2.00 Å and 1.84 Å, while the out-of-plane Mn-O length is 1.98 Å.

[45] P.G. Radaelli *et al.*, Phys. Rev. B **55**, 3015 (1997).

[46] Y. Konishi *et al.*, J. Phys. Soc. Jpn. **68**, 3790 (1999).

[47] Z. Fang, I. V. Solovyev, and K. Terakura Phys. Rev. Lett. **84**, 3169 (2000).

[48] C. W. M. Castleton and M. Altarelli, Phys. Rev. B **62**, 1033 (2000).

[49] Y. Tokura, ed., *Colossal Magnetroresistive Oxides*, Gordon and Breach, New York (2000).

[50] H. Kawano, R. Kajimoto, H. Yoshizawa, Y. Tomioka, H. Kuwahara, and Y. Tokura, Phys. Rev. Lett. **78**, 4253 (1997).

[51] M. v. Zimmermann, J. P. Hill, Doon Gibbs, M. Blume, D. Casa, B. Keimer, Y. Murakami, Y. Tomioka, and Y. Tokura, Phys. Rev. Lett. **83**, 4872 (1999).

[52] J. B. Goodenough, Phys. Rev. **100**, 564 (1955).

[53] Y. Tokura and N. Nagaosa, Science **288**, 462 (2000).

[54] K. H. Ahn, T. Lookman, and A. R. Bishop, Nature **428**, 401 (2004).

[55] Y. Suzuki, H. Y. Hwang, S.-W. Cheong, and R. B. van Dover, Appl. Phys. Lett. **71**, 140 (1997).

[56] Y. Konishi, Z. Fang, M. Izumi, T. Manako, M. Kasai, H. Kuwahara, M. Kawasaki, K. Terakura, and Y. Tokura, J. Phys. Soc. Jpn. **68**, 3790 (1999).

[57] Yoichi Okimoto, Yoshinori Konishi, Makoto Izumi, Takashi Manako, Masashi Kawasaki, and Yoshinori Tokura, J. Phys. Soc. Jpn. **71**, 613 (2002).

[58] Y. Ogimoto, M. Nakamura, N. Takubo, H. Tamaru, M. Izumi, and K. Miyano, Phys. Rev. B **71**, 060403(R) (2005).

[59] Z. Fang, I.V. Solovyev, and K. Terakura, Phys. Rev. Lett. **84**, 3169 (2000).

[60] H. B. Huang, T. Shishidou, and T. Jo, J. Phys. Soc. Jpn. **69**, 2399 (2000); H. B. Huang and T. Jo, *ibid.* **71**, 3094 (2001).

[61] D. J. Huang, W. B. Wu, G. Y. Guo, H.-J. Lin, T. Y. Hou, C. F. Chang, C. T. Chen, A. Fujimori, T. Kimura, H. B. Huang, A. Tanaka, and T. Jo, Phys. Rev. Lett. **92**, 087202 (2004).

[62] F. Iga, M. Tsubota, M. Sawada, H. B. Huang, S. Kura, M. Takemura, K. Yaji, M. Nagira, A. Kimura, T. Jo, T. Takabatake, H. Namatame, and M. Taniguchi, Phys. Rev. Lett. **93**, 257207 (2004).

[63] Douglas B. Chrisey and Graham K. Hubler, ed., Pulsed Laser Deposition of Thin Films, John Willey & Sons, New York (1994).

[64] M. Kawasaki, M. Izumi, Y. Konishi, T. Manako, and Y. Tokura, Materials Science & Engineering B **63**, 49 (1999).

[65] C. T. Chen, F. Sette, Y. Ma, M. S. Hybertsen, E. B. Stechel, W. M. C. Foulkes, M. Schulter, S-W. Cheong, A. S. Cooper, L. W. Rupp, Jr., B. Batlogg, Y. L. Soo, Z. H. Ming, A. Krol, and Y. H. Kao, Phys. Rev. Lett. **66**, 104 (1991).

[66] W. B. Wu, D. J. Huang, J. Okamoto, A. Tanaka, H.-J. Lin, F. C. Chou, A. Fujimori, and C. T. Chen, Phys. Rev. Lett. **94**, 146402 (2005).

[67] In principle, our calculations should be denoted as GGA+U. Nonetheless, following the tradition, we use LDA+U here.[68, 69]

[68] V. I. Anisimov, J. Zaanen, and O. K. Andersen, Phys. Rev. B **44**, 943 (1991).

[69] A. I. Liechtenstein, V. I. Anisimov, and J. Zaanen, Phys. Rev. B **52**, R5467 (1995).